Hindawi
Mobile Information Systems
Volume 2022, Article ID 1420539, 12 pages
https://doi.org/10.1155/2022/1420539

Research Article

A Covariance Matrix-Based Cooperative Spectrum Sensing Algorithm in Electric Wireless Private Network

Xu Zhao,[1] Jie Gan,[1] Weiyang Xu,[2] and Tiancong Huang[2]

[1]*Beijing Smart-Chip Microelectronics Technology Co.,Ltd., Beijing, China*
[2]*School of Microelectronics and Communication Engineering, Chongqing University, Chongqing, China*

Correspondence should be addressed to Tiancong Huang; htc@cqu.edu.cn

Received 10 October 2022; Revised 25 November 2022; Accepted 7 December 2022; Published 21 December 2022

Academic Editor: Juraj Machaj

Cognitive radios can significantly improve the spectral efficiency of wireless communications. Spectrum sensing is a key function of cognitive radios to prevent the harmful interference with licensed users. This paper considers the cooperative spectrum sensing in 230 MHz electric wireless private networks. First, the statistical distribution of the sample covariance matrix of the received signals is investigated. Then, taking the ratio of the sum of absolute values of the off-diagonal elements of the sample covariance matrix to that of the diagonal elements as the decision metric, an improved covariance absolute value (ICAV) cooperative sensing algorithm is proposed. After that, a performance analysis concerning the probabilities of false alarm and detection is carried out. Theoretical analysis and simulation results show that the ICAV algorithm possesses an accurate decision threshold and is robust to the noise uncertainty.

1. Introduction

Wireless communication has been widely applied in the distribution network, enabling the electric vehicle charging, information collection, two-way interactive marketing, and smart grid [1]. On the other hand, the development of a smart grid has put higher requirements on the network structure, coverage, and bandwidth. At present, general packet radio service (GPRS) and code division multiple access (CDMA) are widely used in electric power wireless communication. They are both public network technologies, which do not need to deploy a private network for power services. However, the network security and reliability are inferior to private networks, while the high rental fee paid to telecom operators is another concern [2]. Therefore, the National Committee of China has allocated the 230 MHz frequency band to build a new electric wireless private network (EWPN) called the TD-LTE 230 system. To meet the requirements of intelligent distribution, the TD-LTE 230 system utilizes up-to-date technologies to reduce the transmission latency and improve the spectrum efficiency.

It is worth noting that the 230 MHz EWPN may share the same spectrum with the existing 230 digital radio stations; thus, it is of significant importance to confirm the proper operation of these two systems. Specifically, the cognitive radio that can enable the transceiver to adapt transmit parameters based on its interaction with the environment in which it operates to improve the quality of communications has been considered as a promising technology in 230 MHz EWPN [3]. One of the most critical and challenging tasks in cognitive radio is to sense the presence of licensed users (LUs). Two main purposes of the spectrum sensing are to sense spectrum holes to meet system throughput and quality of service requirements, as well as to ensure that there is no interference to LUs [4]. Based on the above considerations, this paper regards the 230 digital radio stations as the LUs and the EWPN nodes as the secondary users (SUs). If the EWPN nodes detect the presence of 230 digital radio stations, they will not occupy the band so as to avoid interference. Therefore, the spectrum sensing is indispensable to achieve the efficient use of spectrum resources in the environment where 230 digital radio stations and EWPN nodes coexist.

2. Related Work

The existing spectrum sensing algorithms can be generally classified into energy detection (ED), matched filter detection, and feature detection. Energy detection is the most widely used, because of its low complexity, low detection delay, and simplicity to implement. More importantly, it is a blind detection method that does not require prior information of the LU's signals. However, energy detection cannot guarantee the reliability of spectrum sensing in the presence of noise uncertainty [5]. Match filtering detection is known as optimal if the prior information of signals emitted by LUs is known, but in some situations, it is difficult to obtain these information in advance [6]. Feature detection, which relies on the cyclostationary or second-order statistics, is computationally inefficient due to the exploitation of a large number of received symbols for averaging [7]. For example, the eigenvalue-based sensing is known for having a high detection rate without requiring any knowledge about the LU or the noise level [8]. In addition, since the spectrum sensing is essentially a classification problem, data-driven learning technologies have been advocated as a promising solution. In [9], by using its substantial improvement in the classification, a deep reinforcement learning-based spectrum sensing was proposed. Capitalizing on the hierarchical nature of feature extraction in deep neural networks (DNNs), a novel multitask DNN architecture to detect spectrum occupancy was designed in [10].

It is worth noting that the abovementioned spectrum sensing schemes are conducted in a single node, which has the limitation that it is difficult to detect the signals of LUs for desired performance in low signal-to-noise ratio (SNR) conditions [11]. In contrast, a cooperative spectrum sensing has been proposed as a promising solution, which can effectively address issues that arise in spectrum sensing due to noise uncertainty, fading, shadowing, and hidden terminals [12]. In cooperative spectrum sensing, data fusion and the final decision can be executed in two different modes, namely, centralized or decentralized [13]. In the centralized mode, each SU senses the specific spectrum separately and reports the local detection result to the fusion center via a reporting channel. The fusion center analyzes the reported information received from all SUs to make a decision and then sends the result back to SUs. On the other hand, there is no fusion center in the decentralized mode, and each SU makes decisions independently. Considering the limited communication resources between SUs and the fusion center, this paper focuses on the problem of cooperative spectrum sensing in the centralized mode.

A major category of cooperative spectrum sensing exploits the statistical distribution law of random matrix. Specifically, since LU's signals propagate through independent wireless channels to SUs, then each received copy must strongly correlate with each other. Therefore, the detection algorithm based on the sample covariance matrix takes advantage of the correlation among received signals to detect the presence of LU [14]. One benefit of this approach is that it does not require prior information such as channel characteristics and noise variance. For example, a fusion rule based on dynamic grouping was designed to facilitate the distributed cooperative spectrum sensing in heterogeneous cognitive radio networks [11]. Zeng and Liang proposed the covariance absolute value (CAV) sensing algorithm [15]. Yang et al. investigated a detection approach based on the covariance Cholesky factorization (CCF) [16]. More recently, a covariance matrix-aware convolutional neural network-based multiband joint spectrum sensing method was proposed in [17].

2.1. Motivation and Contributions. Although the CAV and CCF algorithms can be applied in the multiuser cooperative sensing scenario, there are some key issues that have not been dealt with. For example, we will show that there is a mismatch between the actual probability distribution function (PDF) of the CAV method and the theoretical one. This discrepancy could result in a loss of detection performance. Moreover, the CCF algorithm is of high complexity due to the requirement of matrix decomposition, which is less efficient in performing spectrum sensing or switching. To avoid the aforementioned problems, we propose a new cooperative spectrum sensing algorithm based on the sample covariance matrix. The major contributions are summarized as follows:

(1) The statistical distribution of the sample covariance matrix of the received signals is investigated. Then, an improved covariance absolute value (ICAV) spectrum sensing algorithm is proposed by taking the ratio of the sum of absolute values of the off-diagonal elements of the sample covariance matrix to that of the diagonal elements as the decision metric.

(2) The performance in terms of the probability of false alarm (Pfa) and the probability of detection (Pd) is analyzed, and their closed-form expressions are obtained. Moreover, the threshold for the cooperative spectrum sensing is derived.

(3) The numerical simulations are performed to verify the effectiveness of our scheme and to investigate the impacts of system parameters on the spectrum sensing accuracy. Moreover, a comparison of the proposed algorithm with the existing ones are obtained.

The rest of the paper is organized as follows: In Section 2, the considered system model is described, including a brief introduction of existing sensing algorithms. In Section 3, the proposed scheme of cooperative spectrum sensing scheme is presented in detail. Section 4 presents the numerical simulation results, based on which the performance analysis and discussion are conducted. Finally, Section 5 concludes this paper.

3. System Model Description

3.1. Scenario of Cooperative Spectrum Sensing. The scenario considered in this paper is centralized cooperative spectrum sensing, as shown in Figure 1. There are K SUs and one LU, as well as a fusion center, where the LU denotes a 230 digital

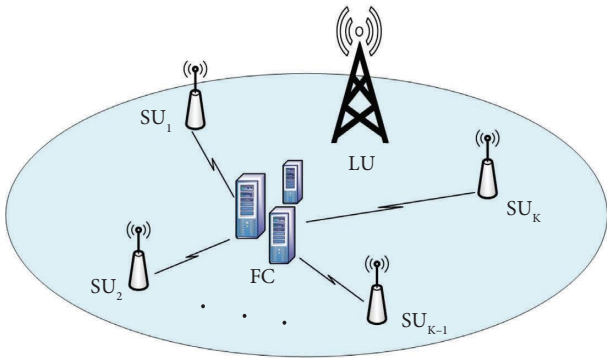

Figure 1: Scenario of cooperative spectrum sensing, where LUs denote the 230 digital radio stations and SUs represent the EWPN nodes.

radio stations and SUs represent EWPN nodes. Specifically, each SU sends the received signals to a fusion center, where the final decision is made and the corresponding results are then broadcast to SUs. Suppose that all SUs participate in spectrum sensing and the number of samples used for averaging is N, then the received signal by the k-th SU at time t is given by the following:

$$y_k(t) = h_k(t)s(t) + w_k(t), \tag{1}$$

where $s(t)$ is LU's signal of zero mean and variance σ_s^2, $h_k(t)$ denotes the channel connecting the LU and the k-th SU, and $w_k(t)$ is the noise component with zero mean and variance σ_w^2. Thus, the SNR is defined as $10\log(\sigma_s^2/\sigma_w^2)$. Moreover, the considered spectrum bandwidth is assumed to be B with central frequency f_c, and the sampling frequency is f_s which satisfies $f_s \geq 2B$. In this paper, we use $y_k(n)$, $s(n)$, $w_k(n)$, and $h_k(n)$ to denote the sampled received signal $y(nT_s)$, transmit signal $s(nT_s)$, noise component $w(nT_s)$, and channel response $h(nT_s)$, respectively. Therefore, the cooperative spectrum sensing can be formulated as a binary hypotheses testing problem, i.e.,

$$y_k(n) = \begin{cases} w_k(n), & H_0, \\ h_k(n)\,s(n) + w_k(n), & H_1. \end{cases} \tag{2}$$

Furthermore, let $\mathrm{y}(n) = [y_1(n), \ldots, y_K(n)]^T$ be the $K \times 1$ signal vector at time instance n, and $\mathrm{Y} = [y(1), \ldots, y(N)]$ indicates the $K \times N$ observation matrix. In a similar way, we employ $\mathrm{w}(n) = [w_1(n), \ldots, w_K(n)]^T$ to denote the $K \times 1$ noise vector, while $\mathrm{W} = [w(1), \ldots, w(N)]$ represents the $K \times N$ noise matrix. Accordingly, the covariance matrix computed by the fusion center is given by the following:

$$\mathrm{R} = E\left\{\mathrm{y}(n)\mathrm{y}^H(n)\right\} = \mathrm{R}_s + \sigma_w^2 \mathrm{I}_K, \tag{3}$$

where R_s is the autocorrelation matrix of LU's signals and I_K denotes the unity matrix of size $K \times K$. Under hypothesis H_0, the covariance matrix is diagonal, whereas it is not diagonal because of the presence of LU's signal under hypothesis H_1.

3.2. The CAV Cooperative Spectrum Sensing Schemes. As aforementioned, the covariance matrix of the received signals is diagonal in the absence of LU, while is nondiagonal in the presence of LU. This observation can be exploited for spectrum sensing, which is the core idea of the CAV method [15]. The decision metric and threshold of the CAV method are as follows:

$$T_{\mathrm{CAV}} = \frac{T_1}{T_2} = \frac{\sum_{i=1}^{K}\sum_{j=1}^{K}\left|r_{ij}\right|}{\sum_{i=1}^{K}\left|r_{ii}\right|}, \qquad \gamma_{\mathrm{CAV}} = \frac{1 + (K-1)\sqrt{2/(N\pi)}}{1 - Q^{-1}\left(P_{fa}\right)\sqrt{2/N}}, \tag{4}$$

respectively. The (i, j)-th element of the sample covariance matrix is denoted by $r_{ij}, 1 \leq i, j \leq K$. P_{fa} denotes the probability of a false alarm, and $Q^{-1}(\cdot)$ indicates the inverse error function. In principle, T_{CAV} equals 1 under hypothesis H_0, whereas $T_{\mathrm{CAV}} > 1$ under hypothesis H_1. Figure 2 compares the analytical threshold and the numerical one, where P_{fa} varies. Obviously, the mismatch between these two curves indicates that the CAV algorithm cannot handle the decision threshold properly. Although this mismatch can be reduced by increasing N, it leads to a poor detection performance, as will be demonstrated later.

4. Proposed Cooperative Spectrum Sensing Algorithm

In practice, the covariance matrix in (3) is not available due to the finite observation samples. On the contrary, the sample covariance matrix $\widehat{\mathrm{R}}$ is used to approximate the true covariance matrix, that is,

$$\widehat{\mathrm{R}} = \frac{1}{N}\mathrm{Y}\mathrm{Y}^H. \tag{5}$$

With sufficient samples, $\widehat{\mathrm{R}}$ can be a good approximation of R. From the analysis above, one can find that the off-diagonal elements of $\widehat{\mathrm{R}}$ describe the correlation among SU's received signals; thus, it is possible to utilize this information to detect the presence of LU's signals. Since $\widehat{\mathrm{R}}$ is a Hermitian matrix, then the sum of the absolute values of its off-diagonal elements and that of diagonal elements are denoted by the following:

$$V_1 = \frac{1}{K}\sum_{i=1}^{K}\sum_{j<i}^{K}\left|r_{ij}\right|, \qquad V_2 = \frac{1}{K}\sum_{i=1}^{K}\left|r_{ii}\right|, \tag{6}$$

respectively. Hence, the decision metric of the proposed algorithm is as follows:

$$T_{\mathrm{ICAV}} = \frac{V_1}{V_2}. \tag{7}$$

We then discuss the differences between T_{ICAV} and T_{CAV}. From Equation (4),we note that T_1 includes T_2, which means there exists a correlation between the numerator and denominator. However, this correlation was ignored when the authors of [16] derived the decision threshold, causing a large

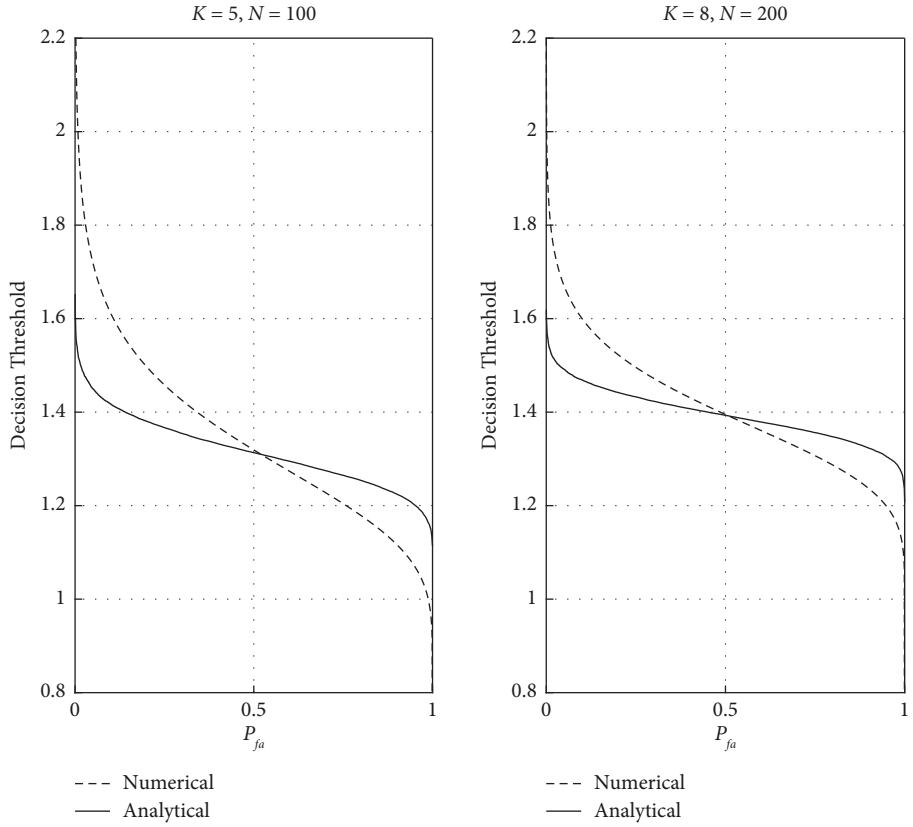

Figure 2: The decision threshold of the CAV algorithm, where the analytical result is obtained by Equation (4).

mismatch between the preset threshold and the actual one. In addition, because of the correlation between T_1 and T_2, the Mellin transform is required to calculate the distribution of T_{CAV}. As a result, the obtained expression of the PDF could be extremely complex. In contrast, the proposed decision metric T_{ICAV} avoids the aforementioned problem since V_1 and V_2 are statistically independent.

The complexity of the proposed ICAV algorithm is mainly attributed to two parts: computation of the sample covariance matrix and the decision metric. The first part requires $N(N+1)K/2$ multiplications and $N(N+1)(K-1)/2$ additions. For the second part, generally, $K(K+1)$ additions are required. As for the CAV algorithm, its complexity is basically the same as the proposed one. On the other hand, the complexity of the CCF-based algorithm also comes from the computation of the sample covariance matrix and decision metric. While the complexity of calculating the sample covariance matrix is identical, that of Cholesky factorization includes about $O(N^3/3)$ multiplications and additions. Note that \$N\$ is usually larger than \$K\$, since more samples of the received signal are beneficial to obtain a more accurate sample covariance matrix. Therefore, the complexity of the CCF-based spectrum sensing is much higher than the proposed ICAV algorithm.

4.1. The PDF and CDF of the Proposed Metric. In this part, the PDF and cumulative distribution function (CDF) of the proposed ICAV algorithm are derived. Assume the noise component $w_k(n)$ is Gaussian-distributed, i.e, $w_k(n) \sim CN(0, \sigma_w^2)$. Under hypothesis H_0, the nondiagonal element $r_{ij}, i \neq j$ can be written as follows:

$$\begin{aligned} r_{ij} &= \frac{1}{N} \mathrm{W}(i,:)\mathrm{W}(:,j) \\ &= \frac{1}{N} \sum_{n=1}^{N} w_i(n) w_j^*(n), \end{aligned} \tag{8}$$

where $\mathrm{W}(i,:)$ and $\mathrm{W}(:,j)$ denote the i-th row and j-th column of W, respectively; $w_i(n)$ is independent of $w_j(n)$. Let us define $z_{ij} \triangleq N r_{ij}$; then, its PDF is as follows:

$$f_{Z_{ij}}(t)=\begin{cases}\dfrac{1}{\sigma_w^2(m-1)!}\exp\left(-\dfrac{|t|}{\sigma_w^2}\right)\displaystyle\sum_{i=0}^{m-1}\frac{(m+i-1)!}{2^{m+i}i!(m-i-1)!}\left(\frac{|t|}{\sigma_w^2}\right)^{m-i-1}, & N=2m,\\ \dfrac{\left(|t|/\left(2\sigma_w^2\right)\right)^m}{\sqrt{\pi}\chi(m+1/2)\sigma_w^2}K_m\left(\dfrac{|t|}{\sigma_w^2}\right), & N=2m+1,\end{cases}\tag{9}$$

where $\chi(\cdot)$ is the Gamma function and $K_m(\cdot)$ is the second kind of modified Bessel function of m. Let $Q_{ij}=|z_{ij}|$; then, its PDF can be derived as follows:

$$f_{Q_{ij}}(t)=\begin{cases}f_{Z_{ij}}(t)+f_{Z_{ij}}(-t), & t>0,\\ 0, & t\le 0.\end{cases}\tag{10}$$

According to Equations (9) and (10), the mean and variance of Q_{ij} are derived by the following:

$$\begin{aligned}u_{Q_{ij}}&=E\left\{Q_{ij}\right\}=\int_{-\infty}^{+\infty}qf_Q(q)dq=\sqrt{\frac{2N}{\pi\sigma_w^2}}\\ \sigma_{Q_{ij}}^2&=D\left\{Q_{ij}\right\}=\int_{-\infty}^{+\infty}q^2f_{Q_{ij}}(q)dq-\left[\int_{-\infty}^{+\infty}qf_{Q_{ij}}(q)dq\right]^2=N\left(\frac{1-2}{\pi}\right)\sigma_w^4.\end{aligned}\tag{11}$$

With Equations (9–11), we can study the distribution of V_1.

According to the definition of V_1, it can be rewritten as follows:

$$\begin{aligned}V_1&=\frac{1}{K}\sum_{i=1}^{K}\sum_{j<i}^{K}\left|r_{ij}\right|,\\ &=\frac{1}{KN}\sum_{i=1}^{K}\sum_{j<i}^{K}\left|Nr_{ij}\right|,\\ &=\frac{1}{KN}\sum_{i=1}^{K}\sum_{j<i}^{K}Q_{ij},\\ &=\frac{1}{KN}\sum_{l=1}^{L}Q(l),\end{aligned}\tag{12}$$

where $Q(l)\subset\left\{Q_{ij}\mid 1\le i\le K,1\le j<i\right\}$, and $L=K(K-1)/2$. Since $Q(l)$ are independent and identically distributed, the mean and variances are $u_{Q_{ij}}$ and $\sigma_{Q_{ij}}^2$, respectively. Therefore, we can obtain that the mean and variance of $Q(l)/(KN)$ are as follows:

$$\begin{aligned}u_{Q_{ij}'}&=\frac{1}{KN}u_{Q_{ij}}=\frac{1}{K}\sqrt{\frac{2}{(N\pi)}}\sigma_w^2\\ \sigma_{Q_{ij}'}^2&=\frac{1}{K^2N^2}\sigma_{Q_{ij}}^2=\frac{1}{K^2N}\left(1-\frac{2}{\pi}\right)\sigma_w^4,\end{aligned}\tag{13}$$

where $Q_{ij}'=Q(l)/(KN)$. When L is sufficiently large, one can arrive at the following result according to the central-limit theorem:

$$\frac{V_1-Lu_{Q_{ij}'}}{\sigma_{Q_{ij}'}\sqrt{L}}\sim N(0,1).\tag{14}$$

Therefore, we have $V_1\sim N\left(Lu_{Q_{ij}'},L\sigma_{Q_{ij}'}^2\right)$, and its PDF and CDF can be given by the following:

$$\begin{aligned}f_{V_1}(t)&=\frac{1}{\sqrt{2\pi L}\sigma_{V_1}}\exp\left(-\frac{\left(t-Lu_{V_1}\right)^2}{2L\sigma_{V_1}^2}\right),\\ F_{V_1}(t)&=\frac{1}{\sqrt{2\pi L}\sigma_{V_1}}\int_{-\infty}^{t}\left(\exp\left(-\frac{\left(t-Lu_{V_1}\right)^2}{2L\sigma_{V_1}^2}\right)\right).\end{aligned}\tag{15}$$

Next, we derive the distribution of V_2. As before, let us assume the elements in W are additive Gaussian noise, namely, $w_k(n)\sim CN(0,\sigma_w^2)$. Then, under hypothesis H_0, we have Y = W; thus, the diagonal elements of the sample covariance matrix are denoted by the following:

$$\begin{aligned}r_{ii}&=\frac{1}{N}\mathrm{W}(i,:)\mathrm{W}(:,i)\\ &=\frac{1}{N}\sum_{n=1}^{N}w_i(n)w_i(n)\\ &=\frac{1}{N}\sum_{n=1}^{N}w_i^2(n).\end{aligned}\tag{16}$$

Meanwhile, according to its definition, V_2 can be written as follows:

$$\begin{aligned} V_2 &= \frac{1}{K}\sum_{i=1}^{K}\left|r_{ii}\right|, \\ &= \frac{1}{K}\sum_{i=1}^{K}\left|\frac{1}{N}\sum_{n=1}^{N}w_i^2(n)\right|, \\ &= \sum_{i=1}^{K}\sum_{n=1}^{N}\left(\sqrt{1/(KN)}\,w_i(n)\right)^2. \end{aligned} \tag{17}$$

From Equation (17), V_2 follows a central chi-square distribution with KN degrees of freedom. Therefore, the k-th moment of V_2 is denoted as follows:

$$E\left\{V_2^k\right\} = \begin{cases} \left(2\sigma_1^2\right)^k \dfrac{\chi(m+k)}{(m-1)!}, & KN = 2m, \\ \left(2\sigma_1^2\right)^k \dfrac{\chi(m+k+0.5)}{\chi(m+0.5)!}, & KN = 2m+1, \end{cases} \tag{18}$$

where $\sigma_1^2 = \sigma_w^2/KN$.

According to the distributions of V_1 and V_2, the CDF and PDF of T_{ICAV} are represented as follows:

$$\begin{aligned} F_{\mathrm{ICAV}}(t) &= P\left(T_{\mathrm{ICAV}} \le t\right), \\ &= P\left(\frac{V_1 - Lu_{Q'}}{\sigma_{Q'}\sqrt{L}} \le \frac{tE(V_2) - Lu_{Q'}}{\sigma_{Q'}\sqrt{L}}\right), \\ &= F_N\left(\frac{\sqrt{2}\,KNt - K(K-1)\sqrt{N/\pi}}{\sqrt{KN(K-1)(1-2/\pi)}}\right), \\ f_{\mathrm{ICAV}}(t) &= \frac{d\left(F_{\mathrm{ICAV}}(t)\right)}{\mathrm{d}t}, \\ &= \frac{\sqrt{2KN}}{\sqrt{(K-1)(1-2/\pi)}} f_N\left(\frac{\sqrt{2}\,KNt - K(K-1)\sqrt{N/\pi}}{\sqrt{KN(K-1)(1-2/\pi)}}\right), \end{aligned} \tag{19}$$

respectively, where $f_N(t) = 1/\sqrt{2\pi}\exp(-t^2/2)$ and $F_N(t) = 1/\sqrt{2\pi}\int_{-\infty}^{t} -t^2/2\mathrm{d}t$ denote the PDF and CDF of a standard Gaussian random variable, respectively, and $E\{V_2\}$ can be computed according to (18). Note that since KN is a large number, $E\{V_2\}$ is obtained by setting $KN = 2m$.

In light of the analysis above, it is observed that V_1 and V_2 are statistically independent of each other, thus making the obtained $F_{\mathrm{ICAV}}(t)$ more accurate. Therefore, it is expected that the preset threshold can match well with the actual one, which will be verified by numerical results.

4.2. The Decision Threshold of ICAV. According to the PDF and CDF of the decision metric and the Neyman–Pearson criterion, the P_{fa} can be calculated by the following:

$$\begin{aligned} P_{fa} &= \Pr\left(T_{\mathrm{ICAV}} > \gamma_{\mathrm{ICAV}} \,\middle|\, H_0\right) \\ &= Q\left(\frac{\sqrt{2}\,KN\gamma_{\mathrm{ICAV}} - K(K-1)\sqrt{N/\pi}}{\sqrt{KN(K-1)(1-2/\pi)}}\right), \end{aligned} \tag{20}$$

where $\Pr(\cdot)$ indicates the event's probability, $Q(t) \triangleq 1/\pi\int_t^{\infty}\exp(-t^2)\mathrm{d}t$ is the error function, and γ_{ICAV} denotes the decision threshold. In general, the decision threshold is set according to the predefined P_{fa}. Given Equations (19) and (20), one can obtain the threshold of the proposed sensing algorithm as follows:

$$\gamma_{\mathrm{ICAV}} = \frac{1}{\sqrt{2KN}}\left(Q^{-1}\left(P_{fa}\right)\sqrt{NK(K-1)\left(1-\frac{2}{\pi}\right)} + K(K-1)\sqrt{\frac{2N}{\pi}}\right), \tag{21}$$

where $Q^{-1}(\cdot)$ is the inverse function of $Q(t)$. From Equation (21), it is observed that, aside from P_{fa}, γ_{ICAV} relates to the number of received samples N and the number of SUs K.

To sum up, the proposed ICAV sensing algorithm includes the following steps:

(1) SUs sample the received signals and send them to the fusion center, where the sample covariance matrix is computed.

(2) We calculate the sum of absolute values of non-diagonal elements of the sample covariance matrix to obtain V_1 and calculate the sum of absolute values of diagonal elements to obtain V_2. Then, the decision metric is obtained.

(3) Given a prerequisite P_{fa} and the PDF of the decision metric under hypothesis H_0, we compute the decision threshold according to (21).

(4) If $\gamma_{\mathrm{ICAV}} \geq T_{\mathrm{ICAV}}$, then the hypothesis H_1 is declared; otherwise, H_0 is declared.

5. Simulation Results and Discussion

In this part, extensive numerical simulations are conducted to verify the performance of the proposed ICAV detection algorithm and a comparison with existing methods is also included. All the results were obtained by averaging over 10,000 independent Monte Carlo runs. The channels between different nodes are assumed to follow the Rayleigh fading model.

5.1. Signal Model of LU. At present, 230 digital radio stations are the most widely used power wireless private network, where the minimum shift keying (MSK) modulation scheme is employed. The MSK modulation is a continuous phase frequency shift keying with a modulation index of 0.5, and its time-domain signal is denoted by the following:

$$s(t) = c(t)\cos\left(2\pi f_c t + \phi_0\right) - d(t)\sin\left(2\pi f_c t + \phi_0\right), \quad (22)$$

where

$$\begin{aligned} c(t) &= \sum_{k=-\infty}^{\infty} c_k q\left(t - kT_s - t_0 - \frac{T_s}{2}\right), \\ d(t) &= \sum_{k=-\infty}^{\infty} d_k q\left(t - kT_s - t_0\right), \\ q(t) &= \cos\left(\frac{\pi t}{T_s}\right). \end{aligned} \quad (23)$$

T_s is the sampling interval, f_c is the operational frequency, and ϕ_0 indicates the initial phase. In the following simulation, we set $f_c = 230\mathrm{MHz}$ and the sampling frequency is $f_s = 153.6\mathrm{KHz}$.

5.2. Results and Discussion. Figure 3 draws the analytical and numerical results of $F_{\mathrm{ICAV}}(t)$ with different (K, N) combinations, where P_{fa} varies. The good match between analytical and numerical curves verifies the correctness of our derivation. Besides, Figure 4 shows how the decision threshold T_{ICAV} varies with P_{fa}. Again, the analytical curve matches well with the numerical one. It is observed that T_{ICAV} reduces if one increases the P_{fa}, which is in accordance to our expectation. Moreover, increasing K or N results in a larger T_{ICAV} subject to the same P_{fa}. To sum up, Figures 3 and 4 demonstrate the effectiveness of our derivation, and then, we focus on the detection performance in the following analysis.

Figure 5 depicts the receiver operating characteristic (ROC) curves of spectrum sensing algorithms, where the ED, CAV, CCF, and fusion rule-based schemes are included for performance comparison. In this figure, the simulation parameters are $K = 8$, $N = 200$, and SNR = −5 dB. In addition, we also account for the noise uncertainty, which is caused by the estimation error of noise variance. However, the noise variance can never be precisely estimated, which results in the noise uncertainty. Technically, the estimated noise variance follows a unit distribution, i.e.,

$$\sigma_w^2 \sim U\left(\frac{\sigma_w^2}{u_c}, \widehat{\sigma}_w^2 u_c\right), \quad (24)$$

where $\widehat{\sigma}_w^2$ is the noise variance estimate and u_c is the noise uncertainty, which is usually represented in dB. First of all, one can find that the proposed ICAV detection scheme performs the best among these schemes. For example, P_d achieves approximately 86% at $P_{fa} = 0.1$. In particular, the ED scheme is inherently sensitive to the noise uncertainty, as it is clearly shown that its performance degrades as the noise uncertainty increases. In contrast, our proposed scheme is immune to this kind of uncertainty.

Figure 6 compares the detection performance of different algorithms when SNR varies, where $K = 8$ and $N = 200$. Specifically, the required SNR for the ICAV algorithm to achieve $P_d = 0.9$ is about −8.2 dB, while that of CCF, CAV, and fusion rule-based schemes is −7.7 dB, −6.2 dB, and −4 dB, respectively. Therefore, the performance gain of ICAV algorithm over CCF, CAV, and fusion rule-based schemes is 0.5 dB, 2 dB, and 4.2 dB, respectively. In addition, it is evident that the ICAV algorithm possesses a higher P_d over the ED method. Since the CCF scheme is of high computational complexity due to the requirement of Cholesky decomposition, the proposed algorithm hits a balance between the detection performance and implementation cost.

Figure 7 analyzes the detection performance of different algorithms when the noise uncertainty varies, where $K = 8$, $N = 200$, and SNR = −5 dB. The left and right subfigures relate to the P_d and P_{fa}, respectively. From the left subfigure, the ICAV algorithm shows robustness to the noise uncertainty as it achieves the best P_d. Also, ICAV, CAV, and CCF schemes witness little performance loss when the noise uncertainly becomes severe. In contrast, the ED method is quiet vulnerable to this problem, although it is simple to implement. On the other hand, the right subfigure shows that the P_{fa} of the ICAV and CCF schemes equals the nominal value of 0.05, while that of the CAV and ED schemes deviates from 0.05. Note that this deviation could harm the detection accuracy.

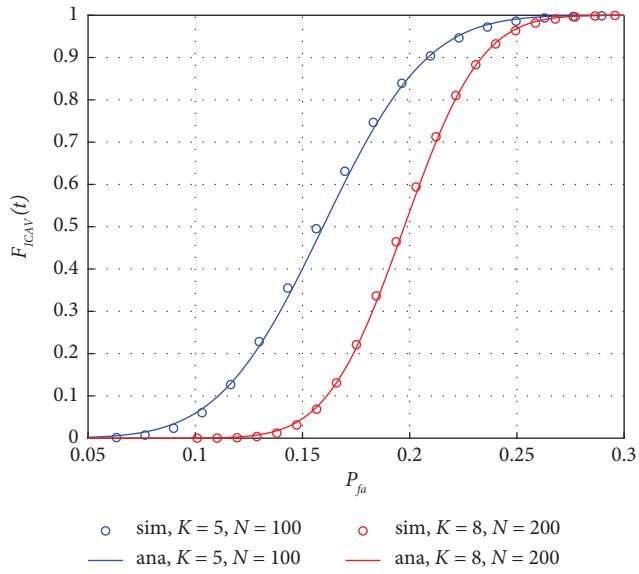

FIGURE 3: The CDF of the decision metric of the proposed ICAV algorithm, where P_{fa} varies.

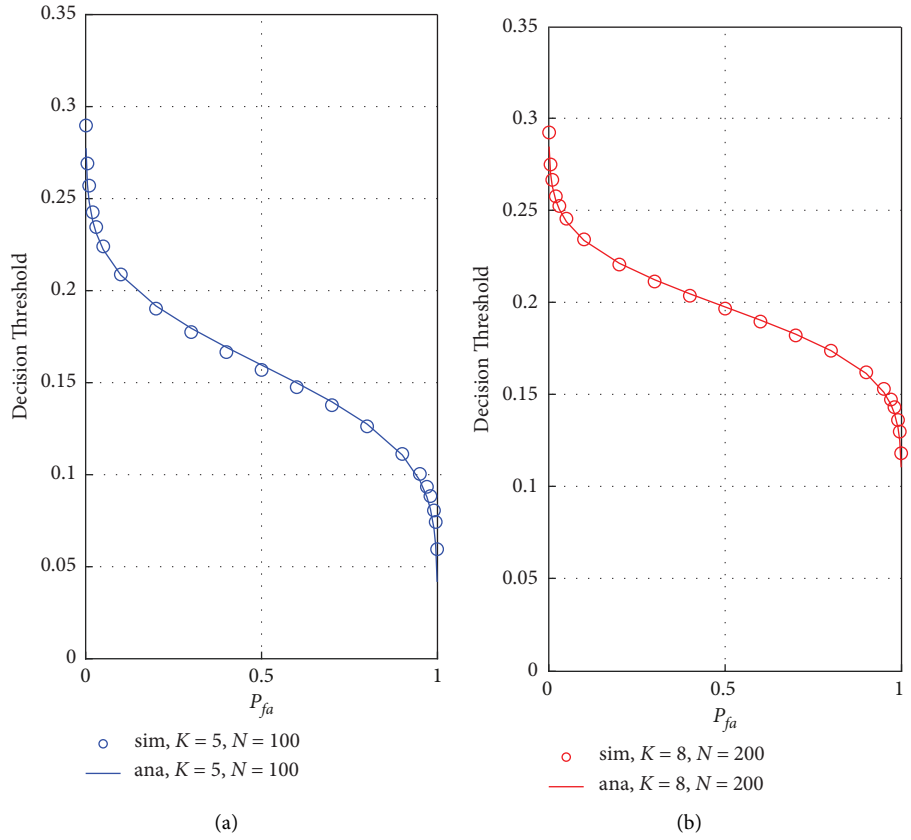

FIGURE 4: The decision threshold of the proposed ICAV algorithm, where P_{fa} varies.

Figure 8 presents the P_d and P_{fa} results when K varies, where SNR = −5 dB, $N = 200$, and the noise uncertainty NU = 0.5 dB. According to the left subfigure, the proposed ICAV algorithm achieves the best detection performance. Besides, the right subfigure shows that the actual P_{fa} of ICAV approximates the nominal value of 0.05, whereas those of other schemes deviate from 0.05 with different extents. Intuitively, the deviation of the ED scheme is caused by its sensitivity to the noise uncertainty, while that of the CAV scheme is due to the mismatch between the analytical threshold and the numerical one shown in Figure 2. Hence, the proposed ICAV scheme is superior to the rest in terms of P_d when the noise uncertainty exists.

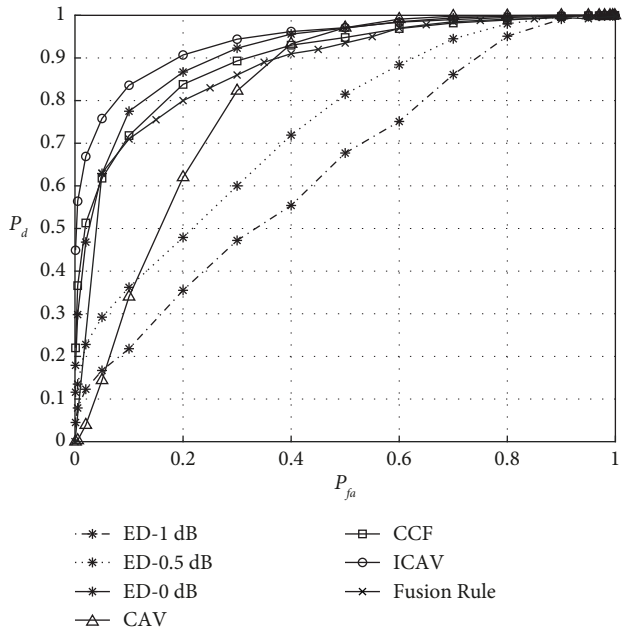

Figure 5: The ROC curves of spectrum sensing algorithms, where the ED, CAV, and CCF schemes are included for performance comparison.

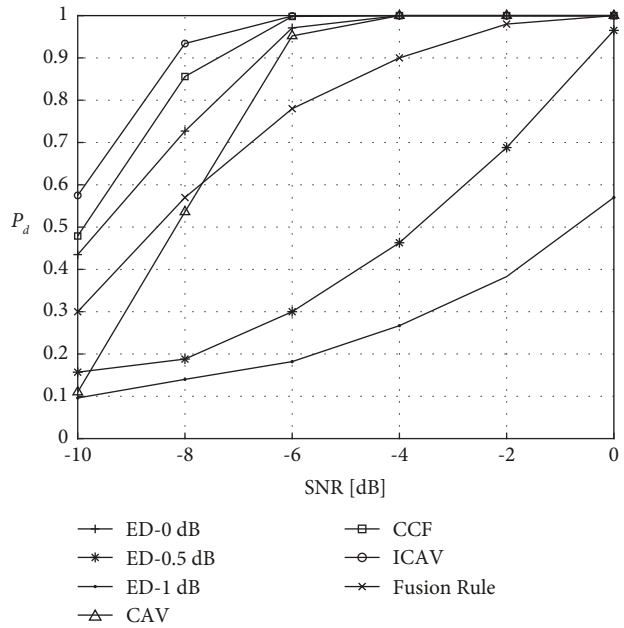

Figure 6: The probability of detection of different algorithms, where SNR varies.

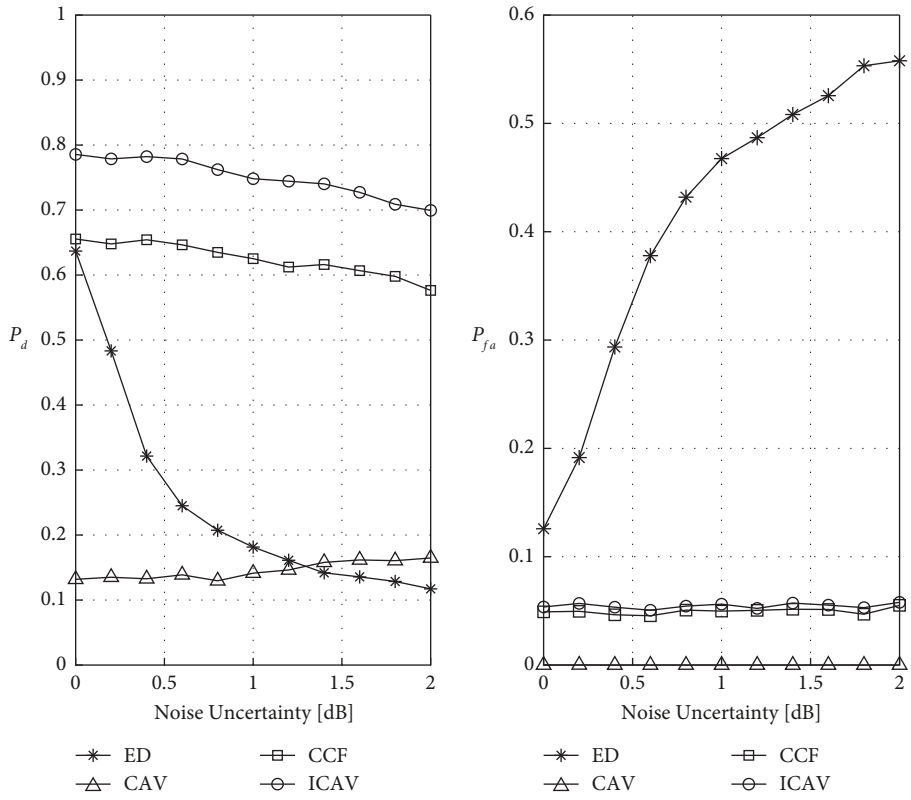

Figure 7: P_d and P_{fa} of different sensing algorithms, where the noise uncertainty varies.

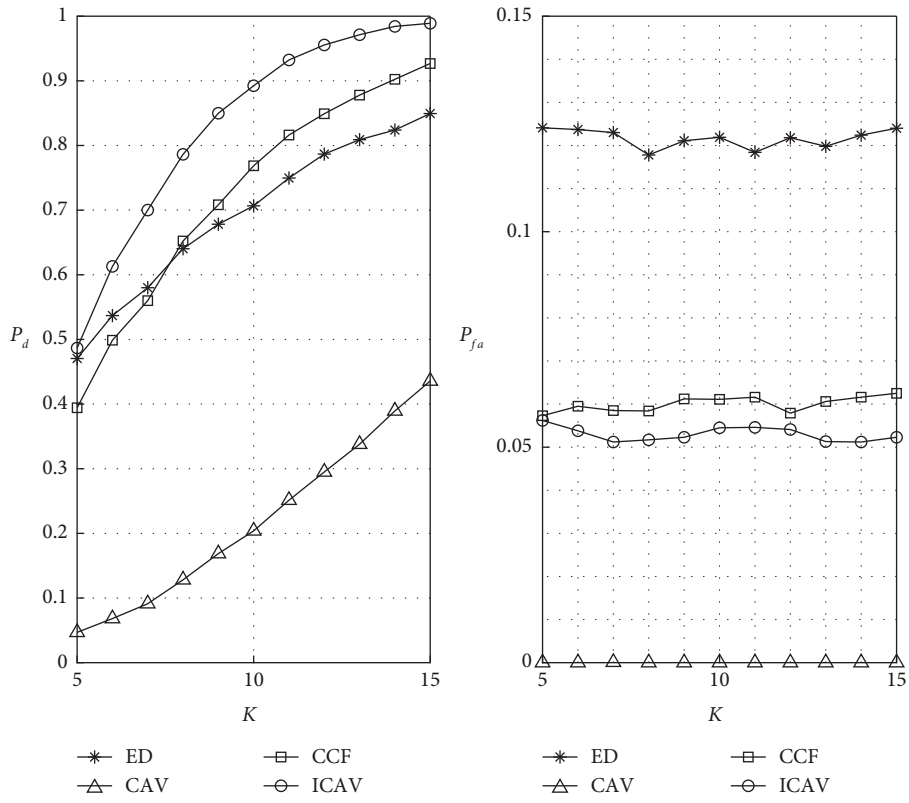

Figure 8: P_d and P_{fa} of different sensing algorithms, where K varies.

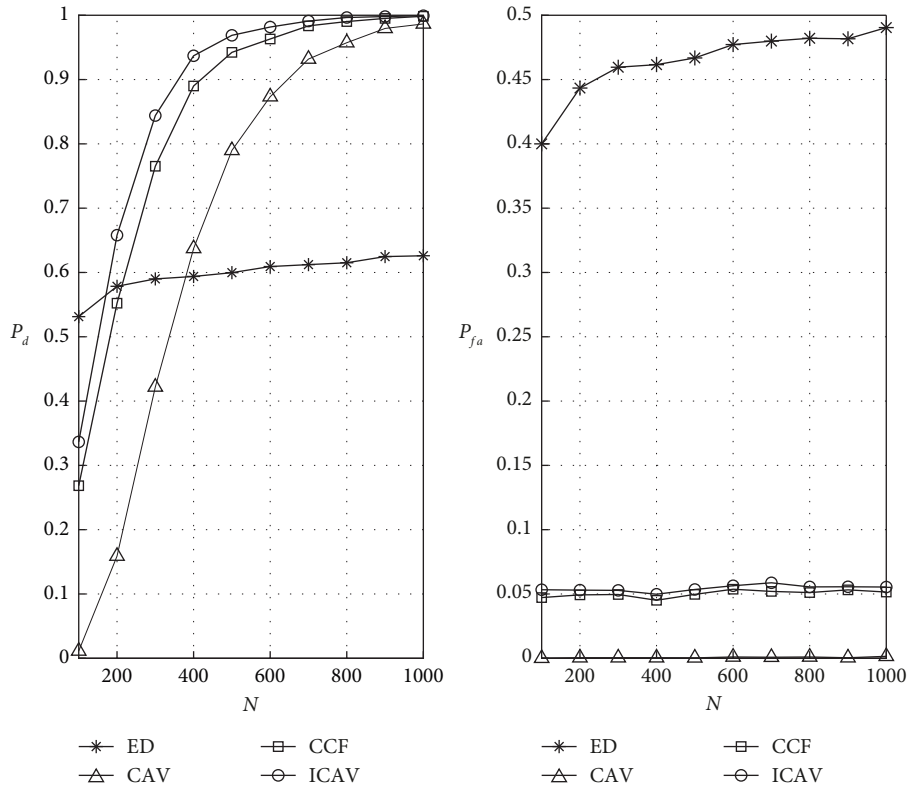

Figure 9: P_d and P_{fa} of different sensing algorithms, where N varies.

Finally, Figure 9 discusses how the performance varies with \$$N$\$, where SNR = −9 dB, $K = 8$, and the noise uncertainty equals to 1 dB. As before, the left and right subfigures consider the P_d and P_{fa}, respectively. For P_d, the proposed ICAV algorithm performs better than the others. The right subfigure indicates that except for the ED method, the rest three achieve a decent performance in terms of P_{fa}. Note that although a larger N is beneficial to improve the detection accuracy, the computational complexity increases as well. Thus, from the system design point of view, one needs to balance between performance and complexity when choosing N.

6. Conclusions

Aiming at the practical problems encountered in the application of the power wireless broadband system, this paper proposed a cooperative spectrum sensing algorithm to realize the coexistence of the newly deployed EWPN system and existing 230-data transmission radio systems. Specifically, through analyzing the statistical distribution of the sample covariance matrix of the received signal, an ICAV spectrum sensing algorithm was proposed. Theoretical analysis and simulation results showed that the proposed ICAV algorithm achieved a more accurate threshold compared to the CAV algorithm. Moreover, the proposed ICAV algorithm not only was robustness to the noise uncertainty but also struck a balance between the detection performance and computational complexity.

Data Availability

The data used to support the findings of this study are available from the corresponding author upon request.

Conflicts of Interest

The authors declare that they have no conflicts of interest.

Acknowledgments

This work was supported by Ultra-low-power, Multi-connection and High-security M2M Communication Chip, the 2020 State Grid Corporation of China Science and Technology Program, under Grant 5700-202041398A-0-0-00.

References

[1] M.-Y. Zhai, "Transmission characteristics of low-voltage distribution networks in China under the smart grids environment," *IEEE Transactions on Power Delivery*, vol. 26, no. 1, pp. 173–180, 2011.

[2] Y. Yan, Y. Qian, H. Sharif, and D. Tipper, "A survey on smart grid communication infrastructures: motivations, requirements and challenges," *IEEE Communications Surveys & Tutorials*, vol. 15, no. 1, pp. 5–20, 2013.

[3] S. Haykin, "Cognitive radio: brain-empowered wireless communications," *IEEE Journal on Selected Areas in Communications*, vol. 23, no. 2, pp. 201–220, 2005.

[4] T. Yucek and H. Arslan, "A survey of spectrum sensing algorithms for cognitive radio applications," *IEEE Communications Surveys & Tutorials*, vol. 11, no. 1, pp. 116–130, 2009.

[5] N. S. Kim and J. M. Rabaey, "A dual-resolution wavelet-based energy detection spectrum sensing for UWB-based cognitive radios," *IEEE Transactions on Circuits and Systems I: Regular Papers*, vol. 65, no. 7, pp. 2279–2292, 2018.
[6] E. Axell and E. G. Larsson, "Optimal and sub-optimal spectrum sensing of OFDM signals in known and unknown noise variance," *IEEE Journal on Selected Areas in Communications*, vol. 29, no. 2, pp. 290–304, 2011.
[7] G. Huang and J. K. Tugnait, "On cyclostationarity based spectrum sensing under uncertain Gaussian noise," *IEEE Transactions on Signal Processing*, vol. 61, no. 8, pp. 2042–2054, 2013.
[8] A. Sabra and M. Berbineau, "Experimental assessment of eigenvalue-based spectrum sensing using USRP-based MIMO testbed for cognitive radio applications," *IEEE Sensors Letters*, vol. 6, no. 10, pp. 1–4, 2022.
[9] R. Sarikhani and F. Keynia, "Cooperative spectrum sensing meets machine learning: deep reinforcement learning approach," *IEEE Communications Letters*, vol. 24, no. 7, pp. 1459–1462, 2020.
[10] W. Zhang, Y. Wang, F. Yu, Z. Qin, X. Chen, and Z. Tian, "Wideband spectrum sensing based on collaborative multi-task learning," in *Proceedings of the 2022 IEEE International Conference on Communications Workshops (ICC Workshops)*, Seoul Korea, May 2022.
[11] T. Yang, Y. Wu, L. Li, W. Xu, and W. Tan, "Fusion rule based on dynamic grouping for cooperative spectrum sensing in cognitive radio," *IEEE Access*, vol. 7, pp. 51630–51639, 2019.
[12] S. Zheng, Y. Jiang, X. Ge, Y. Xiao, Y. Huang, and Y. Liu, "Cooperative spectrum sensing and fusion based on tangle networks," *IEEE Transactions on Network Science and Engineering*, vol. 9, no. 5, pp. 3614–3632, 2022.
[13] Z. Chen, Y.-Q. Xu, H. Wang, and D. Guo, "Federated learning-based cooperative spectrum sensing in cognitive radio," *IEEE Communications Letters*, vol. 26, no. 2, pp. 330–334, 2022.
[14] S. Ma, Y. Wang, J. Ren, and M. Yin, "A cooperative spectrum sensing method based on soft low-rank subspace clustering," *IEEE Transactions on Circuits and Systems II: Express Briefs*, vol. 69, no. 9, pp. 3954–3958, 2022.
[15] Y. Zeng and Y.-C. Liang, "Spectrum-sensing algorithms for cognitive radio based on statistical covariances," *IEEE Transactions on Vehicular Technology*, vol. 58, no. 4, pp. 1804–1815, 2009.
[16] X. Yang, K. Lei, S. Peng, and X. Cao, "Blind detection for primary user based on the sample covariance matrix in cognitive radio," *IEEE Communications Letters*, vol. 15, no. 1, pp. 40–42, 2011.
[17] J. Zhang, Z. Q. He, H. Rui, and X. Xu, "Multiband joint spectrum sensing via covariance matrix-aware convolutional neural network," *IEEE Communications Letters*, vol. 26, no. 7, pp. 1578–1582, 2022.